

Simulation and optimization of an axial impedance pump

Jan Alexander, Joris Degroote, and Jan Vierendeels

Ghent University, Department of Flow, Heat and Combustion Mechanics
Sint-Pietersnieuwstraat 41, B-9000 Ghent, Belgium
Jan.Alexander@UGent.be, Joris.Degroote@UGent.be, Jan.Vierendeels@UGent.be

Abstract

In this research the fluid – structure interaction in a multi layer axial impedance pump is analyzed numerically. The fluid dynamics solver *Fluent* is coupled with the structure mechanics solver *Abaqus*. Based on the results from these simulations the flow rate is optimized as a function of the excitation frequency. The efficiency of the pump at resonance frequency is determined. To investigate the functioning of the pump at resonance frequency both Fourier analysis and wave intensity analysis are used.

Keywords: Valveless pumping, Computational Fluid Dynamics, Fluid Structure Interaction, Computational Structure Mechanics

The multi layer axial impedance pump

The embryonic heart

The human heart is a very complex structure. Yet it develops from a very simple tubular valveless pump. In the earlier embryonic stages of development the blood flow of the vertebrate is driven by a phenomenon that is called the Liebau-effect. In 1954 Gerhart Liebau introduced the principle of the single layer valveless axial impedance pump [9]. This pump consists of a flexible tube in between two stiffer tubes. Liebau, and after him many others, demonstrated that by pinching the tube asymmetrically from the ends a net flow can be induced.

In the same way the embryonic heart is capable of inducing a net positive blood flow by periodical contractions of the artery wall [3]. Forouhar et al. convincingly showed that the driving principle of the blood flow in the heart of a chicken embryo is not the same as the one that forces swallowed food from the mouth to the stomach. It is important to note that the place of contraction is invariable. Therefore the principle behind the embryonic heart is not the peristaltic principle.

Apart from the vertebrate embryonic heart axial valveless pumps can be found in adult *Amphioxiformes* [13] and it has been argued that the adult human heart functions corresponding to the Liebau-effect during cardiopulmonary resuscitation (CPR) [16].

There are two main incentives for the investigation of the axial impedance pump. First there is the medical reason: a better understanding of the flow dynamics in the embryonic heart is interesting since it may help to understand the complex development process of the four-chamber adult heart. Apart from the genetic factors the hemodynamical feedback is expected to play an important role in this for-

mation process.

Second, the axial impedance pump offers a number of interesting technical advantages:

1. Due to the very simple mechanical design that contains no failure-prone components like valves the axial impedance pump offers some interesting possibilities for micro-electronical applications.
2. The strict separation of the fluid and the components of the pump is a very desirable property for pumping systems of bio-fluids.

These two reasons have made that the axial impedance pump has been the subject of many research projects since Liebau's first experiments. The single layer axial impedance pump has already been investigated experimentally [1, 8], analytically [1] and numerically [7].

The biggest disadvantage of the axial impedance pump is the complex control system that is needed. The performance of the pump is extremely sensitive to small changes in the actuation parameters like frequency and duty ratio of pinching. The control of these parameters will not be easy in a practical system.

The pumping principle

In literature two different aspects are recognized as causing the flow. First there is the static asymmetry of the construction, simply due to the fact that the elastic part at one side of the pincher is longer than at the other side a net flow in the direction of the longest elastic part originates. Bringley et al. [1] demonstrated that by neglecting the frequency influence completely a net flow can be calculated, much like the *valveless diffuser pump* investigated by Olsson et al. [11]. Just like the valveless diffuser pump uses the difference in flow resistance between a nozzle and a diffuser to obtain a net positive flow without using valves the axial

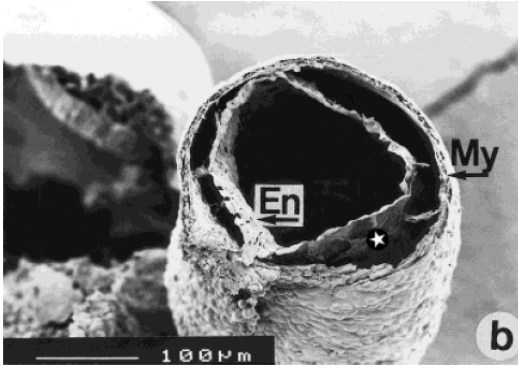


Figure 1 The embryonic heart of a chicken [14]

impedance pump uses the difference in flow resistance between the longer flexible part and the shorter flexible part. Secondly there is clear evidence that resonance plays a strong role in the functioning of the axial impedance pump. All researchers report a very clear non-linear relation between the actuation frequency and the mass flow through the pump.

The idea behind the multi layer axial impedance pump is that one can enforce the resonant waves in the structure by preventing the tube to expand outward. The construction is only slightly more complex. The outer part of the tube is stiffer, thus preventing the thick inner gel-like layer to expand outward. The goal is to maximize the inward wave. Loumes investigated this pump using a monolithic code [10]. The idea is based on the the structure of the embryonic heart of a mammal. Figure 1 shows the embryonic heart of a chicken embryo. One can see that there is a stiffer outside layer (indicated with *My* from *Myocardium*) and a gel-like inner layer (indicated with a '*', it is called the cardiac jelly).

The model

The model is composed of two main parts: the fluid domain that is simulated using the CFD¹-solver FLUENT and the structure domain that is simulated using the CSM²-solver ABAQUS. Both parts are coupled using the IQN-ILS algorithm. This is a technique that solves the said equations at the interface using quasi-Newton iterations with an approximation for the residual's Jacobian matrix using a least-squares model [2]. In this section four things will be discussed: first the geometrical parameters of the model, then the characteristics of the fluid domain and the structure domain and finally the IQN-ILS algorithm that was used to couple both.

Geometry

Due to the axi-symmetrical geometry of the three dimensional multi layer axial impedance pump the numerical model could be constructed in two dimensions. A model was constructed with dimensions similar to the dimensions used by Loumes [10] and Hickerson [6] (see figure 2 and

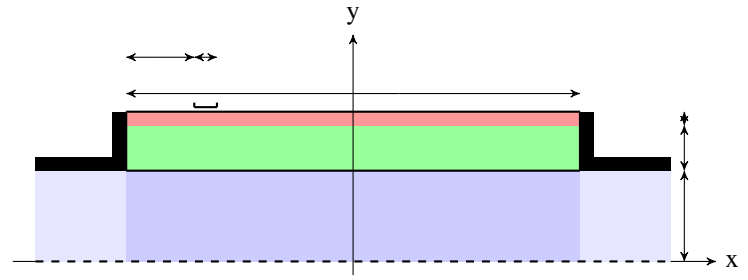


Figure 2 Model of the multi layer axial impedance pump.

Geometry	
Length	0.152 m
Radius fluid domain	0.0055 m
Pincher clearance from end of tube	0.016 m
Pincher width	0.010 m
Thickness inner layer	0.00405 m
Thickness outer layer	0.00075 m
Fluid	
Density	1000 $\frac{kg}{m^3}$
Viscosity	0.003 $\frac{Ns}{m^2}$
Structure	
Density	1000 $\frac{kg}{m^3}$
Stiffness inner layer	5000 Pa
Stiffness outer layer	10 ⁶ Pa
Poisson coefficient inner layer	0.3
Poisson coefficient outer layer	0.49

Table 1 Geometrical and physical parameters of the model

table 1). This way it was hoped to be able to compare with the results of these different researches.

Fluid

The used flow equations are the well known conservation laws for incompressible Newtonian fluid:

$$\vec{\nabla} \cdot \vec{v}_f = 0 \quad (1)$$

$$\frac{\partial \vec{v}_f}{\partial t} + \rho_f \vec{\nabla} \cdot (\vec{v}_f \vec{v}_f) = \rho_f \vec{f}_f + \vec{\nabla} \cdot \vec{\tau}_f \quad (2)$$

these are the expressions for the conservation of mass and momentum. In these equations the fluid velocity is \vec{v}_f , ρ_f is the fluid density, \vec{f}_f is the body force on the fluid and $\vec{\tau}_f$ is the viscous stress tensor of the fluid.

The discretization of these equations (first order in both time and space) by the fluid solver introduces a discretization error. It is important to find a compromise between minimizing these effects by using a finer grid and a smaller time step and keeping the calculation time manageable. To accord both factors in a sensible way a number of tests were run. For these tests a growing running wave was imposed

¹Computational Fluid Dynamics

²Computational Structure Mechanics

on the fluid-structure interface. This wave has an amplitude of 40% of the original fluid diameter in the middle of the tube and amplitude decreasing to zero for places closer to the ends of the tube. It grows in amplitude in a time of 0.1s and moves with a velocity of $1.72 \frac{m}{s}$. This is represented in figure 3. The comparison of the performance of the different simulations was done based on the mass flow in and out and the pressure in a point on the interface close to the middle of the tube.



Figure 3 Deformation of the fluid domain under prescribed motion of fluid-structure interface

Two things could be learned from these tests. First is that due to the large deformation of the fluid domain a Laplace-equation based grid adaption system is needed. The grid moves based on the solution of the following Laplace-equations:

$$\begin{cases} \vec{\nabla}^2 u_x = \Delta u_x = 0 \\ \vec{\nabla}^2 u_y = \Delta u_y = 0 \end{cases} \quad (3)$$

where $\vec{u} = [u_x \ u_y]^T$ is the displacement of the grid vertices in two dimensions.

Secondly it could be decided that the solution of the fluid simulation is more sensitive to the time-step than to the grid (see figures 4 and 5). For the number of time steps it was decided to use simulations with 100 time steps per period in the exploring calculations of the process but for the more accurate simulations more time steps per period have been used.

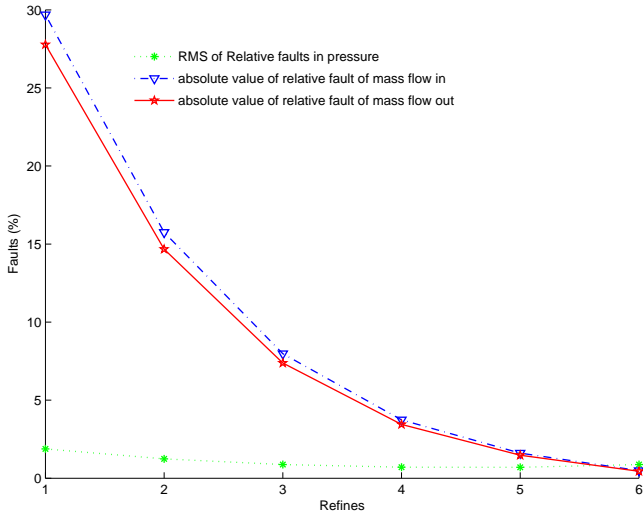


Figure 4 Faults relative to the simulation with the smallest time step of simulations with a different number of time steps per period

Structure

The deformation of the structure is determined by the conservation of momentum

$$\rho_s \frac{d^2 \vec{d}_s}{dt^2} = \rho_s \vec{f}_s + \vec{\nabla} \cdot \vec{\tau}_s \quad (4)$$

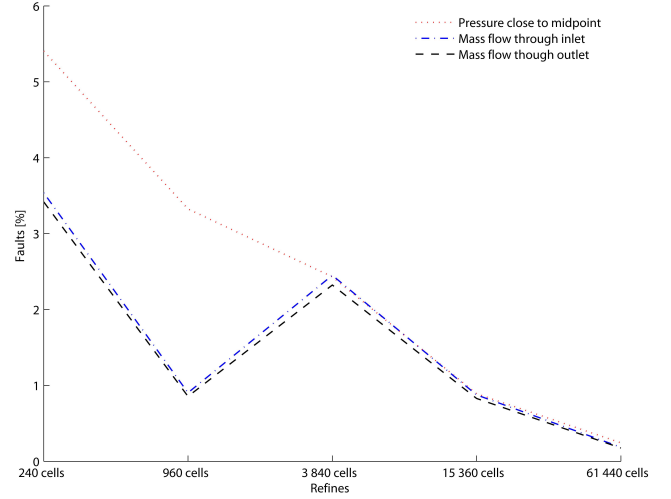


Figure 5 Relative faults with relation to the simulation with the finest grid

where ρ_s is the density of the structure material and \vec{f}_s is the body force per unit volume of the structure. The displacement of the structure is \vec{d}_s and $\vec{\tau}_s$ is the stress tensor.

The structure domain is composed of three parts. First there is the outer thin stiff layer, then there is the thicker inner flexible layer of the tube. The final component of the structure domain is the pincher.

The pincher is a separate component of the structure domain. The other, and less computationally expensive option of implementing the contraction by simply defining the movement of a part of the outer surface of the tube caused unwanted phenomena. By actively defining the movement of this part of the structure to be zero between two pinches it was observed that the pressure waves in the structure reflected at the edges of this part. Between pinches there should be no physical difference between two separate places on the outer surface of the structure domain. For this reason the pincher was modeled using a contact problem in ABAQUS. The movement of the pincher is described by the following equation:

$$y_p(t) = -\frac{A}{2} (1 - \cos(\omega t^*)) \quad (5)$$

The meaning of the different symbols used in these equations are listed in table 2 and in the list of equations 6³.

$$\begin{cases} \omega &= \frac{1}{DR} 2\pi f \\ T &= \frac{1}{f} \\ A &= A_p + d_o \\ t^* &= t - \lfloor \frac{t}{T} \rfloor T \end{cases} \quad (6)$$

The contact between the pincher and the tube was modeled as a *surface-to-surface* contact problem with *finite sliding* contact tracking. Because of the use of a contact problem it was not possible to use 8-node cells, 4-node cells were used instead. Secondly the damping of the structure

³The floor of a: $\lfloor a \rfloor = \max \{m \in \mathbb{Z} | m \leq a\}$

Symbol	Meaning
y_p	Position of the pincher
f	Pinching frequency
DR	Duty Ratio of pinching (40%)
A_p	Pinching amplitude (1mm)
d_o	Pinching offset (0,1mm)
t	Time
T	Pinching period

Table 2 Meaning of the symbols used in equation 6

was modeled to be 8% using Rayleigh β -damping. This means that the factor $\beta = 0,00367$ in

$$\underline{C} = \beta \underline{K} \quad (7)$$

is chosen such that $\zeta = \frac{\beta}{2}\omega = 8\%$ where \underline{C} is the damping matrix of the structure and \underline{K} is the elasticity matrix. $\omega = 43,4Hz$ is the lowest eigenfrequency of the structure without contact with the fluid.

In the same ways as for the fluid domain tests were performed to assess the influence of the simulation parameters on the simulation of the structure domain. For these tests the total kinetic energy and the total strain energy present in the complete structure were compared. It could be concluded that for the structure simulation the time step was not that critical. In ABAQUS the convergence of the simulation is aided by splitting each time step in smaller *time increments*⁴. It is sufficient to use 50 increments and 100 time steps per period. The influence of the grid is more important. A grid with 100 length segments can only be used for exploring calculations. For more accurate results 200 length segments are needed, it is not practical to use more than 200 length segments because then the simulation time becomes too long.

Coupling algorithm

The axial impedance pump is a fluid–structure interaction problem. To couple the fluid solver and the structure solver (Fluent and Abaqus) the IQN-ILS algorithm is used [2]. This coupling algorithm solves the fixed point formulation of the interface problem using quasi-Newton iteration using an approximation of the inverse of the residuals Jacobian matrix from a least-squares model.

At the interface between the fluid domain and the structure domain two conditions have to be met. First there is the kinematic condition: the displacement of the interface in the structure solver \vec{d}_s and the displacement in the fluid solver \vec{d}_f must be equal.

$$\vec{d}_f = \vec{d}_s \quad (8)$$

Secondly there is the dynamic condition: the stress on the interface calculated by both solvers has to be equal.

$$\vec{n}_f \cdot \vec{\tau}_f = -\vec{n}_s \cdot \vec{\tau}_s \quad (9)$$

⁴It should be noted that this is not the case in FLUENT. The number of time increments only influences the ABAQUS-simulation, not the FLUENT-simulation.

In equation 9 $\vec{\tau}$ is the stress tensor and \vec{n} is the unit normal vector pointing outwards from the fluid domain and the structure domain. The conditions that have to be met inside both of the domains were already described: these are the equations of conservation of mass and momentum in the fluid domain and the conservation of momentum in the structure domain.

Now the formulation of this problem can be simplified considerably. With x the displacement of the entire fluid-structure boundary and y the stress load (pressure + shear stress) on it we can write the flow solver \mathcal{F} and the structure solver \mathcal{S} in fixed point notation.

$$y = \mathcal{F}(x) \quad (10)$$

$$x = \mathcal{S}(y) \quad (11)$$

and in the root finding formulation

$$f(x, y) = \mathcal{F}(x) - y = 0 \quad (12a)$$

$$s(x, y) = \mathcal{S}(y) - x = 0 \quad (12b)$$

Then the residual of the FSI problem can be defined as

$$\mathcal{R}(x) = \mathcal{S} \circ \mathcal{F}(x) - x \quad (13)$$

where $\mathcal{S} \circ \mathcal{F}(x) = x$ represents the complete FSI-problem.

Solving equation 13 can be done by using Newton-Raphson iterations:

$$\left. \frac{\partial \mathcal{R}}{\partial x} \right|_{x^k} \Delta x = -r^k \quad (14a)$$

$$\Delta x = x^{k+1} - x^k \quad (14b)$$

where the residual is calculated as

$$r^k = \mathcal{R}(x^k) = \mathcal{S} \circ \mathcal{F}(x^k) - x^k = \tilde{x}^k - x^k \quad (15)$$

To solve equation 14a the Jacobian matrix of \mathcal{R} needs to be known. Since FLUENT and ABAQUS are black box solvers this information is not available. In [15] a technique to approximate a Jacobian of a function based on sets of inputs and outputs of this function has been introduced. Still, if the Jacobian of \mathcal{R} is approximated, it is necessary to solve the linear system 14a. It is more advantageous to approximate the inverse of the Jacobian. It is not necessary to approximate the inverse of the Jacobian of \mathcal{R} explicitly, it is sufficient to estimate the product of this matrix with the vector $\Delta r = 0 - r^k = -r^k$.

$$x^{k+1} = x^k + \left(\widehat{\left. \frac{\partial \mathcal{R}}{\partial x} \right|_{x^k}} \right)^{-1} \Delta r \quad (16)$$

In quasi-Newton iteration k flow and structural equation are solved resulting in $\tilde{x}^k = \mathcal{S} \circ \mathcal{F}(x^k)$ and the corresponding residual r^k . These $\Delta r^{k-1} = r^k - r^{k-1}$ and $\Delta \tilde{x}^{k-1} = \tilde{x}^k - \tilde{x}^{k-1}$ are then stored in the columns of the matrices $\underline{V}^k \in \mathbb{R}^{p \times q}$ and $\underline{W}^k \in \mathbb{R}^{p \times q}$.

$$\underline{V}^k = \begin{bmatrix} \Delta r^{k-1} & \Delta r^{k-2} & \dots & \Delta r^1 & \Delta r^0 \end{bmatrix} \quad (17a)$$

$$\underline{W}^k = \begin{bmatrix} \Delta \tilde{x}^{k-1} & \Delta \tilde{x}^{k-2} & \dots & \Delta \tilde{x}^1 & \Delta \tilde{x}^0 \end{bmatrix} \quad (17b)$$

These matrices can than be combined with those from previous time steps

$$\underline{\underline{V}}'^k = \begin{bmatrix} \underline{\underline{V}}^k & n\underline{\underline{V}} & \dots & n-r+2\underline{\underline{V}} & n-r+1\underline{\underline{V}} \end{bmatrix} \in \mathbb{R}^{p \times v} \quad (18a)$$

$$\underline{\underline{W}}'^k = \begin{bmatrix} \underline{\underline{W}}^k & n\underline{\underline{W}} & \dots & n-r+2\underline{\underline{W}} & n-r+1\underline{\underline{W}} \end{bmatrix} \in \mathbb{R}^{p \times v} \quad (18b)$$

This can have a very positive influence on the convergence, however it is possible that if information from too many time steps is reused the convergence is slowed down, because it is possible that information from time step $n - r + 1$ is not longer relevant in the present time step.

Now the vector $\Delta r = -r^k$ can be approximated by a linear combination of the known Δr^i in matrix $\underline{\underline{V}}'^k$.

$$\Delta r \approx \underline{\underline{V}}'^k \alpha^k \quad (19)$$

with $\alpha \in \mathbb{R}^{v \times 1}$ the vector of coefficients of the decomposition. Since generally $p \leq v$ this is an overdefined set and the least squares solution is calculated. For this purpose the QR-decomposition of $\underline{\underline{V}}'^k$ is calculated ($\underline{\underline{Q}}^k$ is an orthogonal matrix and $\underline{\underline{R}}^k$ an upper triangular matrix)

$$\underline{\underline{V}}'^k = \underline{\underline{Q}}^k \underline{\underline{R}}^k \quad (20)$$

$$\begin{aligned} \underline{\underline{Q}}^k &\in \mathbb{R}^{p \times v} \text{ with } \underline{\underline{Q}}^k [\underline{\underline{Q}}^k]^T = \underline{\underline{I}} \text{ and } [\underline{\underline{Q}}^k]^T \underline{\underline{Q}}^k = \underline{\underline{I}} \\ \underline{\underline{R}}^k &\in \mathbb{R}^{v \times v} \end{aligned}$$

Now α^k can be determined by solving the triangular system

$$\underline{\underline{R}}^k \alpha^k = [\underline{\underline{Q}}^k]^T \Delta r \quad (21)$$

Because it is possible that one of the Δr^i is (almost) a linear combination of other columns of $\underline{\underline{V}}'^k$ these small elements have to be detected and if one is present, the corresponding columns of $\underline{\underline{V}}'^k$ en $\underline{\underline{W}}'^k$ have to be removed. Otherwise the equation corresponding to that row of $\underline{\underline{R}}^k$ cannot be solved during the back substitution.

Now the $\Delta \tilde{x}$ corresponding to Δr can be calculated

$$\Delta \tilde{x} = \underline{\underline{W}}'^k \alpha^k \quad (22)$$

from equation 15 it follows that $\Delta r = \Delta \tilde{x} - \Delta x$. Substitution of equation 22 finally results in

$$\Delta x = \underline{\underline{W}}'^k \alpha^k - \Delta r. \quad (23)$$

Equation 23 can be seen as a procedure to calculate the product of the approximation of the inverse of the Jacobian and a vector $\Delta r = -r^k$ since it allows for Δx to be approximated for a given Δr .

$$\Delta x = \widehat{\frac{\partial \mathcal{R}}{\partial x}} \Big|_{x^k} \Delta r = \underline{\underline{W}}'^k \alpha^k + r^k \quad (24)$$

It can be proven that for the part of Δr that is in the span of the columns of $\underline{\underline{V}}'^k$ Newton iterations are performed while Gauß-Seidel iteration are used for the part of Δr perpendicular to $\underline{\underline{V}}'^k$. Since two vectors are needed to form the matrix $\underline{\underline{V}}'^k$, a relaxation with factor ω is used in the second iteration of the first time step (or, if no information from previous time steps is used the second iteration of every time step).

Fluid structure interaction

Tests have been performed to assess the influence of the simulation parameters on the whole model. Special attention has been given to the top of the pressure wave on the interface because one of the objectives was to get an idea of the numerical dissipation. This is illustrated in figure 6. In figure 7 the result of such an analysis is represented, it becomes clear that a relatively high number of time steps is necessary for the simulations. As a practical maximum 400 time steps per period is accepted. Based on this investigation the conclusions that were drawn from the tests on the structure domain and on the fluid domain separately were confirmed.

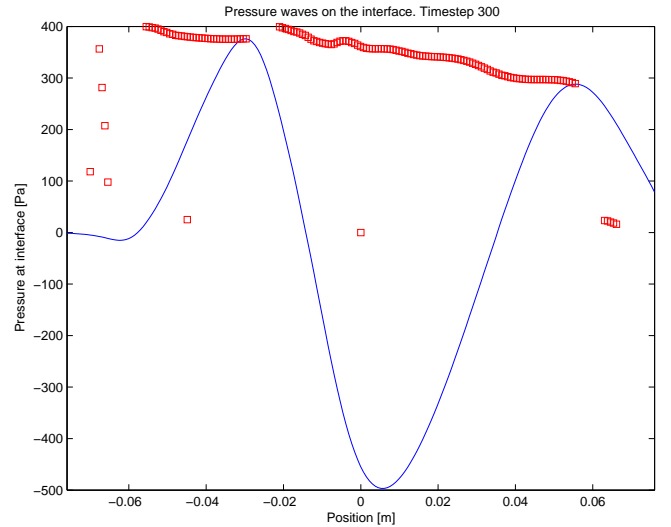


Figure 6 Illustration of the algorithm used to track the top of the pressure wave

The optimization

First the model described in the last section was optimized for mass flow with respect to frequency using an iterative method. Then this optimal frequency was investigated further.

The optimization was done in three steps.

In the first step the most interesting region was determined using 4 period simulations with a coarse grid and a low number of time steps per period. The mesh of the fluid domain consisted of 50×10 elements and the grid of the structure domain consisted of 100×12 linear elements.

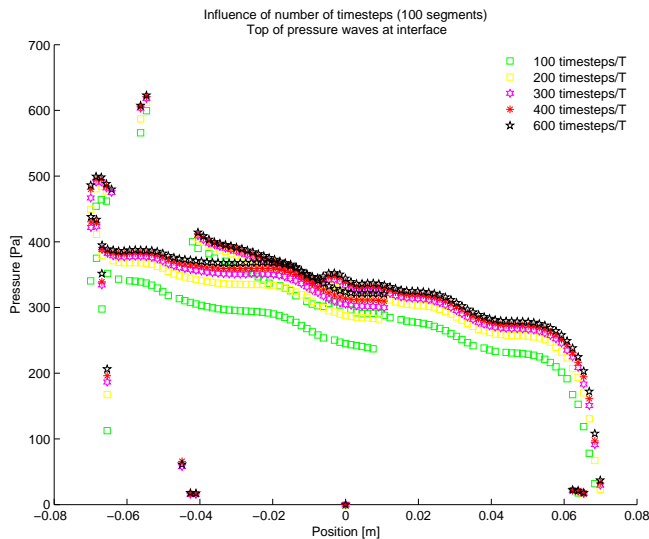


Figure 7 Result of the following of the top of the wave for simulations with a different number of time steps per period and a grid with 100 segments in the length.

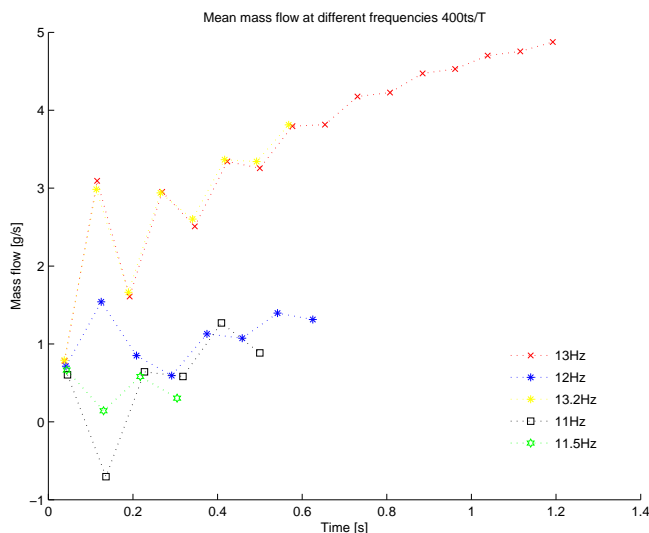


Figure 8 Optimization of the model

The number of ABAQUS increments was set to 50 for 100 time steps per period. It is clear that these parameters do not offer optimal accuracy but they allow for manageable duration of simulation.

In a second step the number of simulated periods is increased to 8 periods, the size of the grid and the time step size stays the same. In this step the presumption was confirmed that the highest mass flow was obtained for the actuation frequency $f = 13Hz$.

In the last step of the optimization process the grid was changed to a 200×10 grid in both the structure domain and the fluid domain. The number of time increments per time steps in ABAQUS was always between 40 and 120. Per period 400 time steps were done. Thus the numerical errors were brought to a minimum within practical possibilities of calculation time. After 16 periods steady state is not yet fully attained. It is clear though that the mass flow of $80 \frac{g}{s}$

Loumes reported [10] from another numerical research will not be attained, nor will the $20g/s$ Hickerson [4] reports. The main reason for this might be that the pinching duty ratio percentage of the period the pincher is actually moving) is a lot higher than the duty ratio of 10% that was used by Loumes. Hickerson already reported the strong impact of the duty ratio for the single layer axial impedance pump. It was attempted already to use a duty ratio of 20% but this did not result in better performance, this does not mean however that it is useless to do a more elaborate study of the influence of the duty ratio.

Analysis

Energetic

The analysis of the axial impedance pump was done. First the energetic analysis of the pump is performed based on the 14th period. It becomes clear that there are two problems that negatively influence the energy performance of the pump. First of all the power delivered by the pincher to the system is not very large. A lot of the power ‘flows back’ to the pincher when the structure exercises force on the retracting pincher. A second problem is that although the energy is well distributed between the structure and the fluid⁵ the energy that is transported to the fluid is not well converted in pumping power.

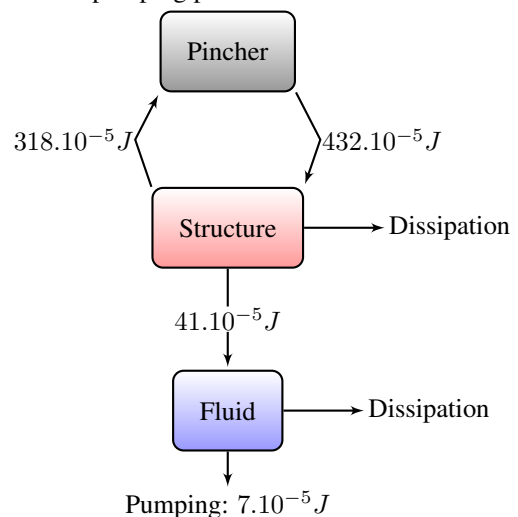


Figure 9 Symbolic representation of the energy flow from the pincher to the fluid

Wave intensity analysis

Wave intensity analysis is a analysis technique based on the method of Riemann characteristics [12]. For this technique one dimensional equations are used that are derived from the conservation of mass and momentum in an elastic vessel. The pressure waves (static pressure p) on the centerline and velocity waves (axial velocity u) on the centerline in this vessel are described as the summation of successive wavefronts that propagate forward and backward through the vessel.

⁵since the density of both is the same one can only expect the energy in both to be of the same order of magnitude

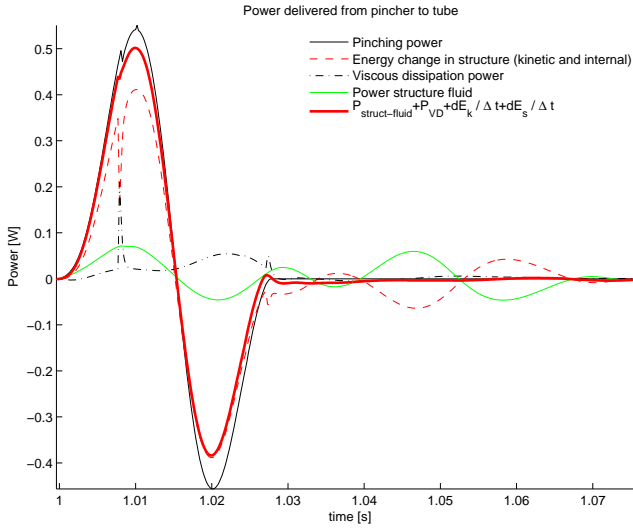


Figure 10 Energetic analysis of the 14th period

The concept of a wavefront

It is very common in science and engineering to think about a wave as a sinusoidal wave train, which is the basis of the Fourier analysis method. For this technique however one has to think of a wave more as a solitary wave where several wavelets or wavefronts combine to form the observed wave. The technological developments just before world war II (planes, rockets) called for a way to solve the problems that arise when the Mach number becomes larger than unity (supersonic and hyper supersonic problems). There was a need for a technique to describe the propagation of a single shock wave.

The method of characteristics

The method of characteristics is a mathematical method introduced by Riemann to reduce a hyperbolic partial differential equation to a family of ordinary differential equations along which the solution can be integrated. The partial differential equations that we will use this method on here are the Euler formulations of the conservation laws in the one dimensional elastic tube. For this analysis only the inviscid, incompressible case is treated.

For a differential element of the tube the law of conservation of mass demands that the change in volume of this element is equal to the net volumetric influx in this element.

$$\frac{\partial A}{\partial t} = -\frac{\partial uA}{\partial x} \quad (25)$$

In these equations A is the area of the tube's cross section. The expression for the conservation of momentum is

$$\frac{\partial u}{\partial t} + \frac{\partial}{\partial x} \left(\frac{u^2}{2} \right) = -\frac{1}{\rho} \frac{\partial p}{\partial x}. \quad (26)$$

By adding that the cross-sectional area of the tube can be written both as a function directly of x and t and as a

function of p and x where p is a function of x and t itself one can easily write an expression for the partial derivatives of A :

$$\begin{aligned} A(x, t) &= A(p(x, t), x) \\ &\Rightarrow \\ \begin{cases} \left(\frac{\partial A}{\partial x} \right)_t &= \left(\frac{\partial A}{\partial p} \right)_x \frac{\partial p}{\partial x} + \left(\frac{\partial A}{\partial x} \right)_p \\ \left(\frac{\partial A}{\partial t} \right)_x &= \left(\frac{\partial A}{\partial p} \right)_x \frac{\partial p}{\partial t} \end{cases} \quad (27) \end{aligned}$$

Using equations 27 the system can be rewritten.

$$\begin{cases} \frac{\partial p}{\partial t} + u \frac{\partial p}{\partial x} + \frac{A}{\left(\frac{\partial A}{\partial p} \right)_x} \frac{\partial u}{\partial x} &= -u \left(\frac{\partial A}{\partial x} \right)_p \\ \frac{\partial u}{\partial t} + \frac{1}{\rho} \frac{\partial p}{\partial x} + u \frac{\partial u}{\partial x} &= 0 \end{cases}$$

The matrix of the coefficients of the x -derivative terms is

$$\begin{bmatrix} u & \frac{A}{\left(\frac{\partial A}{\partial p} \right)_x} \\ \frac{1}{\rho} & u \end{bmatrix}$$

and has got the following eigenvalues: $\lambda_{\pm} = u \pm \sqrt{\frac{A}{\rho \left(\frac{\partial A}{\partial p} \right)_x}}$.

Where the square root term has got the dimension of velocity. It is the wave speed defined by Bramwell and Hill.

$$c = \sqrt{\frac{A}{\rho} \left(\frac{\partial p}{\partial A} \right)_x} \quad (28)$$

This means that we can write the eigenvalues as $\lambda_{\pm} = u \pm c$. What Riemann observed is that these eigenvalues define the so-called *characteristic directions*. He found that if these eigenvalues are real for a hyperbolic system of equations, then the total derivative with respect to the time simplifies considerably.

$$\frac{d}{dt} = \frac{\partial}{\partial t} + \frac{dx}{dt} \frac{\partial}{\partial x} = \frac{\partial}{\partial t} + (u \pm c) \frac{\partial}{\partial x}$$

Which means that the conservation equations can be rewritten, we obtain ordinary differential equations.

$$\begin{cases} \frac{dp}{dt} - (u \pm c) \frac{\partial p}{\partial x} + u \frac{\partial p}{\partial x} + \rho c^2 \frac{\partial u}{\partial x} &= -u \left(\frac{\partial A}{\partial x} \right)_p \\ \frac{du}{dt} - (u \pm c) \frac{\partial u}{\partial x} + \frac{1}{\rho} \frac{\partial p}{\partial x} + u \frac{\partial u}{\partial x} &= 0 \end{cases} \quad (29)$$

From system 29 ordinary differential equations along the characteristics can be obtained. These equations can be written in a very elegant manner by defining Riemann variables $R_{\pm} \equiv u \pm \int \frac{dp}{\rho c}$

$$\frac{du}{dt} \pm \frac{1}{\rho c} \frac{dp}{dt} = -\frac{uc}{A} \left(\frac{\partial A}{\partial x} \right)_p \quad (30)$$

$$\frac{dR_{\pm}}{dt} = \mp \frac{uc}{A} \left(\frac{\partial A}{\partial x} \right)_p \quad (31)$$

This equation illustrates the peculiar but very favorable result of the method of characteristics: along the characteristics $(u \pm c)$ the partial differential equation can be solved

for the Riemann variables by integrating an ordinary differential equation in time.

The beauty of this result is that, notwithstanding the difficult mathematical operations necessary to reach it, the physical interpretation is very intuitive. If one considers a uniform vessel, $u = 0$ and $\left(\frac{\partial A}{\partial x}\right)_p = 0$ and perturbrates this at $t = 0$ then the Riemann variables remain constant along the characteristics that propagate upstream with speed $+c$ (or rather in positive direction) and downstream with speed $-c$. It is clear that the name *wave speed* makes perfect sense for this c . If $u \neq 0$ the waves propagate upstream and downstream with speed $u \pm c$. Perturbation waves are carried away by the flowing fluid, if you throw a stone in a flowing river you can see the ripples getting carried along with it. If $u \geq c$ information does not travel upstream any more.

To study what is happening at a particular location x at time t we have to find the waves that intersect at (x, t) , then we can find u and p from the values of the Riemann variables R_{\pm} . Firstly the path of the wave depends on the local velocity and the local velocity depends on the waves arriving there. Secondly the wave speed depends on p , so we have to solve integral equations to find p and u from the values of R_{\pm} .

In this work we avoid these mathematical problems by assuming that c is constant. Then the expressions for p and u become quite simple.

$$p = \frac{\rho c}{2} (R_+ - R_-) \quad (32)$$

$$u = \frac{1}{2} (R_+ + R_-) \quad (33)$$

Intensity of a wave

The wave intensity method uses the theoretical results obtained in the method of characteristics to study traveling waves in vessels. In this study the concept *intensity of a wave* dI is very useful and important.

From the definition of the Riemann variables we take the difference equation and solve this for du and dp .

$$dR_{\pm} = du_{\pm} \frac{dp}{\rho c} \Rightarrow \begin{cases} dp = \frac{\rho c}{2} (dR_+ - dR_-) \\ du = \frac{1}{2} (dR_+ + dR_-) \end{cases} \quad (34)$$

Now we define the wave intensity dI at a point x as the product of dp and du .

$$dI(t) = \frac{dp(t) \cdot du(t)}{dt \cdot dt} = \frac{1}{4} \frac{\rho c}{dt^2} (dR_+^2 - dR_-^2) \quad (35)$$

The wave intensity has got the very useful property that forward waves have a strictly positive contribution and backward waves have a strictly negative contribution. Thus, if $dI(t) > 0$ the forward waves at (x, t) are bigger than the backward waves, and vice versa. This means that by measuring dp and du at a single site you can get information about the wave phenomena in the vessel.

The dimension of dI is $\frac{W}{m^2}$ and reflects the energy per unit area carried by the wave as it propagates. The fact that we can split dI means that we can assess the importance of backward and forward waves at any time.

Water hammer equation

Equation 34 results in another very interesting relationship. Not only is it possible to split dI in a positive part dI_+ and a negative part dI_- that correspond with respectively a forward and a backward wave, it is also possible to split du and dp in parts du_+ , dp_+ , du_- and dp_- . To do this we make use of an expression called the *water hammer equation*. If you pass from one forward characteristic to another du and dp are bound by the backward characteristic that intersects the two forward characteristic, this results into equation 36a. In the same way the differences between the Riemann variables in a backward wave are found, this results in equation 36b.

$$dR_- = 0 = du_+ - \frac{dp_+}{\rho c} \quad (36a)$$

$$dR_+ = 0 = du_- - \frac{dp_-}{\rho c} \quad (36b)$$

Equations 36a and 36b give us the water hammer equations or the Joukowski equations.

$$dp_{\pm} = \pm \rho c du_{\pm} \quad (37)$$

The water hammer equation is a simple but useful expression that expresses how closely p and u are linked to each other. A change in u will result in a change in p , this is illustrated by the water hammer effect that gave the water hammer equation its name. If a pipe with flowing water is suddenly closed this can cause a sudden pressure build up in the pipe starting at the valve. The sudden decrease in speed u causes p to rise, if the pipe is closed instantly the pressure rise is given by integrating the Joukowski equation.

$$\Delta p = \rho c \Delta u \quad (38)$$

Using wave intensity analysis in this work

The results of the preceding analysis are used in two different ways to study the axial impedance pump. It is used to estimate the wave speed c in the tube using the loop method and the functioning of the pump is studied by separation of the forward and backward waves.

The wave speed in the tube was calculated using equation 28, the Bramwell-Hill definition of c . The water hammer equation 37 allows a very elegant calculation of the wave speed. If backward waves are absent all changes in p and u are caused by forward waves. This means that the water hammer equation results in a linear relationship between p and u .

$$dp = \rho c du \quad (39)$$

This means that p is a linear function of u when only one type of waves is present in a system (during a certain time interval). Equation 39 allows the wave speed to be calculated if the density ρ of the fluid is known, c is simply the slope of the straight pu -curve. Since this c is exactly the Bramwell-Hill wave speed this allows a consistency check of the study.

The wave speed was assessed in three ways:

1. Using the pu -loop method
2. Using the Bramwell-Hill equation
3. With the algorithm to track the top of the pressure wave on the centerline

All three methods resulted in wave speeds very close to $2,25 \frac{m}{s}$. This speed corresponds to $f(l + a_l + a_w)$ with f the frequency, l the length of the tube, a_l the clearance of the pincher from the end of the tube and a_w is the width of the tube. This gives a strong indication of the close link between the wave speed and the resonance frequency.

The second way Wave Intensity analysis is used in this work is for the visualisation of the fluid waves on the centerline by calculating the wave intensity function dI . Without it interpretation of figure 11 would be practically impossible. By calculation the wave intensity figure 12 can be obtained.

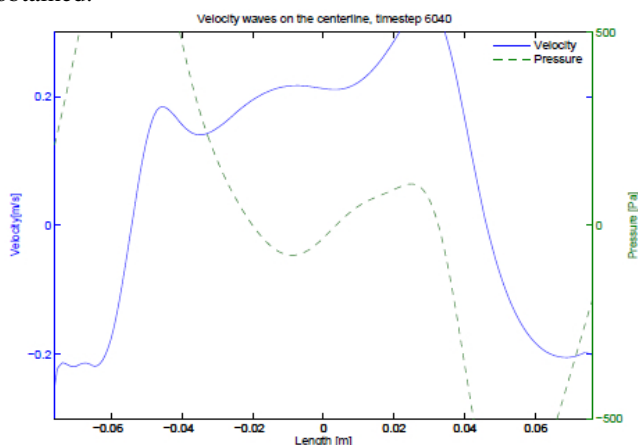


Figure 11 Pressure and velocity wave on the centerline at timestep 6040

Fourier analysis

A second, and far more well-known, way to analyze wave phenomena is the Fourier-method. In this work time-varying spatial waves were investigated. To do this the following procedure was followed:

1. The intensity of the Fourier-components of the wave form in each time step is calculated. This gives a list of wave numbers with corresponding amplitude.
2. These lists are compared for all time steps and the two most important wave numbers over the complete range of time steps are selected. The spatial waves corresponding with these wave numbers are followed over the time span.

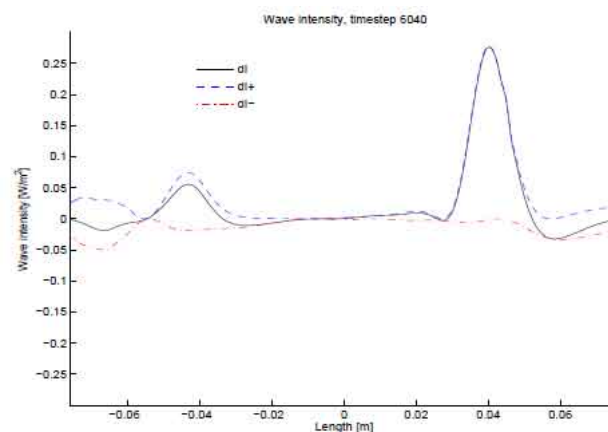


Figure 12 Visualisation of the wave intensity dI on the centerline at timestep 6040

Using this technique it became clear that the wave numbers corresponding to the second and fourth harmonic of the length are the most important. By looking at figure 13 one can see that there is a slight hint of a standing wave in this figure⁶ certainly in comparison with figure 14, this is again a strong indication of the importance of the frequency of actuation.

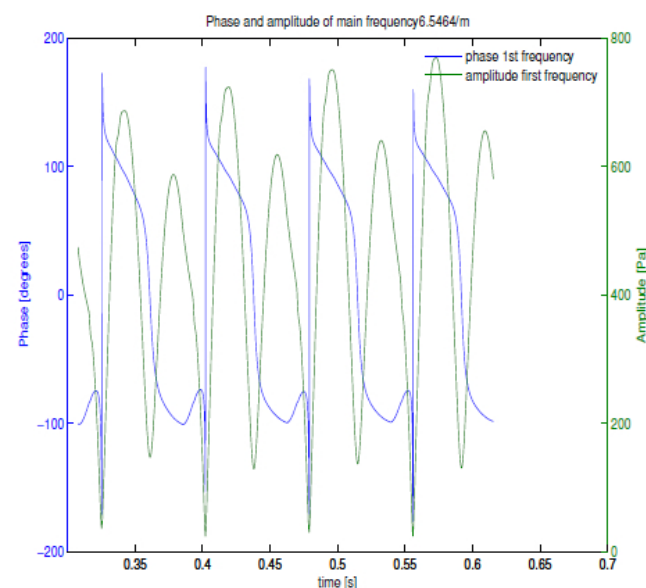


Figure 13 Phase and amplitude of the component with the most important wave number for $f = 13Hz$

Furthermore the high amplitude of the higher wave numbers indicate that these play a role of importance in the functioning of the pump.

Conclusion and suggestions for further investigation

Conclusions about the numerical model parameters

The number of time steps per period and the number of grid cells needed are quite high. Although the average

⁶for a standing wave the frequency would be a square wave and the amplitude a $abs(sin)$ -function

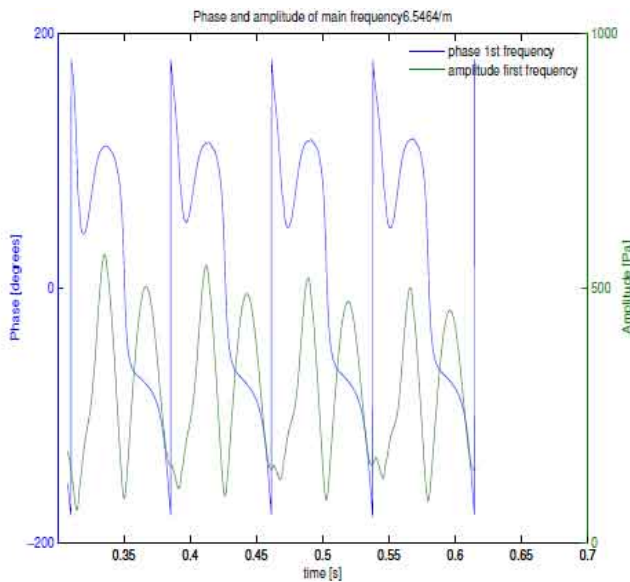


Figure 14 Phase and amplitude of the component with the most important wave number for $f = 12Hz$

mass flow is reasonably well represented by a grid that is coarser (100 length segments) and a lower number of time steps (100 time steps per period) the amplitude of the mass flow function is not well represented by these simulations. This means these simulations can only be used in ‘exploring’ simulations. The accuracy of the simulations can be improved by increasing the number of time steps per period to 400 time steps per period and by making the grid finer to 200×10 in both the structure and the fluid domain. The high number of time steps and the fine grid that is needed make the simulation time high.

Conclusions about the physical parameters and suggestions for further research

Even though a clear net positive flow was observed in this study the contrast between the low mass flow that is found in this work and the higher mass flows that were reported by others [5, 10] suggests that also with this model it should be possible to attain better results.

One of the most promising elements to investigate is whether the performance could be improved by decreasing the duty ratio, as suggested by the results of Hickerson [5].

A high number of parameters on the multi layer axial impedance pump remain to be investigated. The width of the pincher is reported to have a linear effect on the mass flow [5], if the volume displaced by the pincher is increased by 10%, so will the mass flow. Surprisingly, to the best of our knowledge, there has been little investigation on the place of pinching. It is clear that the tube has to be pinched away from the center of the tube but there is no investigation on the influence of the place of pinching on the pumping performance.

Furthermore the influence of the geometrical parameters of the tube should be investigated like the diameter to length ratio or the thickness and flexibility of both the flexible and

the stiff layer.

Acknowledgments

J. Degroote gratefully acknowledges a post-doctoral fellowship of the Research Foundation of Flanders (FWO).

References

- [1] T. T. Bringley, S. Childress, N. Vandenberghe, and J. Zhang. An experimental investigation and a simple model of a valveless pump. *Physics of Fluids*, 20(3):033602–+, Mar. 2008.
- [2] J. Degroote, K.-J. Bathe, and J. Vierendeels. Performance of a new partitioned procedure versus a monolithic procedure in fluid-structure interaction. *Computers & Structures*, 87(11-12):793 – 801, 2009. Fifth MIT Conference on Computational Fluid and Solid Mechanics.
- [3] A. S. Forouhar, M. Liebling, A. Hickerson, A. Nasiraei-Moghaddam, H.-J. Tsai, J. R. Hove, S. E. Fraser, M. E. Dickinson, and M. Gharib. The Embryonic Vertebrate Heart Tube Is a Dynamic Suction Pump. *Science*, 312(5774):751–753, 2006.
- [4] A. Hickerson, D. Rinderknecht, and M. Gharib. Experimental study of the behavior of a valveless impedance pump. *Experiments in Fluids*, 38:534–540, 2005. 10.1007/s00348-005-0946-z.
- [5] A. I. Hickerson. *An Experimental Analysis of the Characteristic Behaviors of an Impedance Pump*. PhD thesis, California Institute of Technology, 2005.
- [6] A. I. Hickerson and M. Gharib. *Journal of Fluid Mechanics*, 555:141–148, 2006.
- [7] E. Jung, S. Lim, W. Lee, and S. Lee. Computational models of valveless pumping using the immersed boundary method. *Computer Methods in Applied Mechanics and Engineering*, 197(25-28):2329 – 2339, 2008. Immersed Boundary Method and Its Extensions.
- [8] G. Liebau. Die Strömungsprinzipien des Herzens. *Zeitschrift für Krieslaufforschung*, 44:677–683, September 1955.
- [9] G. Liebau. Die Bedeutung der Trägheitskräfte für die Dynamik des Blutkreislaufs. *Zeitschrift für Krieslaufforschung*, pages 428–438, December 1956.
- [10] L. Loumes. *Multilayer impedance pump: a bio-inspired valveless pump with medical applications*. Phd thesis, California Institute of Technology, Pasadena, California, December 8th 2006.
- [11] A. Olsson, G. Stemme, and E. Stemme. A numerical design study of the valveless diffuser pump using a lumped-mass model. *Journal of Micromechanics and Microengineering*, 9(1):34, 1999.
- [12] K. Parker. An introduction to wave intensity analysis. *Medical and Biological Engineering and Computing*, 47(2):175–188, Feb. 2009.
- [13] E. Schuit. Valveless impedance pump behavior an experimental study, 2007.
- [14] D. Sedmera, T. Pexieder, N. Hu, and E. B. Clark. Developmental changes in the myocardial architecture

of the chick. *The Anatomical Record*, 248:421–432, February 1997.

- [15] J. Vierendeels, L. Lanoye, J. Degroote, and P. Verdonck. Implicit coupling of partitioned fluid-structure interaction solvers using reduced-order models. *Computers and Structures*, 85(11-14):970–976, 2007.
- [16] J. Werner, H. Greene, C. Janko, and L. Cobb. Visualization of cardiac valve motion in man during external chest compression using two-dimensional echocardiography. implications regarding the mechanism of blood flow. *Circulation*, 63:1417–1431, 1981.